Langmuir

Article

pubs.acs.org/Langmuir

Nanoparticle Permeation Induces Water Penetration, Ion Transport, and Lipid Flip-Flop

Bo Song, Huajun Yuan, Sydney V. Pham, Cynthia J. Jameson, and Sohail Murad*

Department of Chemical Engineering, University of Illinois at Chicago, 810 South Clinton Street, Chicago, Illinois 60607, United States

ABSTRACT: Nanoparticles are generally considered excellent candidates for targeted drug delivery. However, ion leakage and cytotoxicity induced by nanoparticle permeation is a potential problem in such drug delivery schemes because of the toxic effect of many ions. In this study, we have carried out a series of coarse-grained molecular dynamics simulations to investigate the water penetration, ion transport, and lipid molecule flip-flop in a protein-free phospholipid bilayer membrane during nanoparticle permeation. The effect of ion concentration gradient, pressure differential across the membrane, nanoparticle size, and permeation velocity have been examined in this work. Some conclusions from our studies include (1) The number of water molecules in the interior of the membrane during the nanoparticle permeation increases with the nanoparticle size and the pressure differential across the membrane but is unaffected by the nanoparticle permeation velocity or the ion concentration gradient. (2) Ion transport is sensitive to the size of nanoparticle as well as the ion concentration gradient between two sides of the membrane; no anion/cation selectivity is observed for small nanoparticle permeation, while anions are preferentially translocated through the membrane when the size of nanoparticle is large enough. (3) Incidences of lipid molecule flip-flop increases with the size of nanoparticle and ion concentration gradient and decreases with the pressure differential and the nanoparticle permeation velocity.

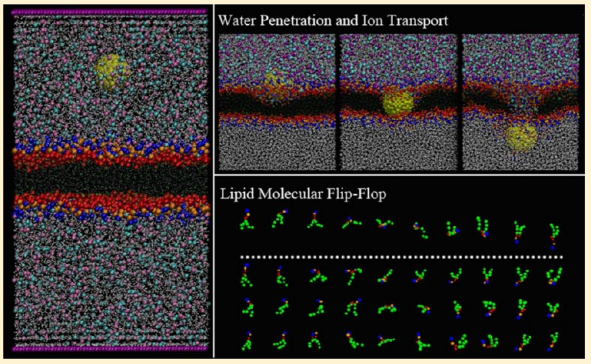

1. INTRODUCTION

Biological membranes are one of the major structural elements of cells, which play a key role as selective barrier and substrate for many proteins that facilitate transport and signaling processes. These selective permeable membranes define the boundary and maintain the essential intracellular environment of the cell. Small molecules such as Xe, O_2, and CO_2 can diffuse across the cell membranes; however, water molecules and ions, such as Na^+, Ca^{2+}, Cl^-, may not easily permeate the cell membranes on their own.[1] Although water penetration and ion transport in living cells are mainly governed by specific water and ion channels, lipid membranes themselves are not perfect barriers. Instead, water molecules, ions and other hydrophilic molecules have been observed to leak passively in small amounts across a membrane.[2,3] This passive permeation of water molecules and ions is a highly concerted process in which solvent, ion and the pore formation in the membrane are coupled.[4] Such ion leakage and water transport have attracted significant attention because functioning membranes strive to maintain the ionic electrochemical gradient in a variety of activities such as ATP synthesis and transport of nutrients.

Transport of nanoparticles across biological membranes is of significance in separations, bioimaging, pharmacological applications, and drug delivery systems. Engineered nanoscale particles allow the possibility of affecting biological processes at a fundamental level. At the same time, the ability of these nanoscale particles to enter and be transported within biological bodies in ways that larger particles cannot could have adverse toxicity effects.[5−7] Pore formation in membranes during the permeation of nanoparticles has been reported experimentally recently.[8] It has been suggested that water-conducting pores, which appear in the membrane as defects, can provide a pathway for the translocation of ions.[9−16] Ion leakage and cytotoxicity induced by nanoparticle permeation is a potential problem in drug delivery schemes because of the toxic effect of many ions. Although molecular dynamics simulations[17−25] and dissipative particle dynamics (DPD) simulations[26,27] have been carried out for nanoparticles in lipid bilayers, water penetration and ion transport during the permeation of nanoparticles has not been investigated systematically previously. Some important unanswered questions include the following. How many water molecules and ions may leak during nanoparticle permeation? How do water and ion leakages depend on the physical properties of the nanoparticle (size, shape, permeation velocity)? What if the surrounding environment changes, such as pressure gradient or concentration gradient between two sides of the membrane? How do individual lipid molecules in the immediate vicinity respond when nanoparticle, water, and ions permeate simultaneously? The study of nanoparticle permeation mediated water and ion transport through the cell

Received: July 17, 2012
Revised: November 19, 2012
Published: November 21, 2012

membranes is inherently challenging due to the complexity of the system. Therefore, there is a clear need for physical insight that can help address these and other questions. In a larger context, it would be of interest to determine how the nature of such transport and the interactions between lipid membrane and nanoparticles, in particular, may determine the biocompatibility and toxicity of nanoparticles.

Molecular dynamics (MD) is a powerful tool which can provide structural and dynamic details of the permeation process that are not readily available experimentally. Some molecular dynamics simulations studies have been conducted on pore-formation coupled to ion permeation, water penetration, and lipid flip-flop in the lipid membrane systems recently.[9−13] In nearly all the previous simulations, the pore formation was induced by an electric field or ionic imbalance between two sides of the membrane. For example, Kandasamy and Larson systematically changed the potential difference across the bilayers by explicitly varying the number of anions and cations in the two water compartments. At a large enough charge imbalance, dielectric breakdown occurs, leading to the formation of water pores in the bilayers. Anions and cations then translocate through the pore.[12] Gurtovenko et al. also studied water and ion transport in the protein-free lipid membranes driven by transmembrane ionic charge imbalance.[12,13] Gurtovenko et al. explored the lipid flip-flop mechanism induced by a transmembrane ion density gradient.[28] Tepper et al. simulated the permeation of protons and ions across the lipid membrane by calculating the potential of the mean force for the proton and ion of interest as a function of its position in the membrane.[10]

In our previous work, we investigated the permeation characteristics of bare nanoparticles and ligand-coated nanoparticles across model lipid membranes.[17,18] We also examined the response of the membrane in terms of the structural and mechanical properties of the lipid membrane under the perturbation of nanoparticles. We have observed the formation of transient pores in the membrane during nanoparticle permeation, which motivated us to investigate comprehensively ion transport and water penetration phenomena induced by nanoparticle permeation. In this work, we monitor water molecules in the membrane, ion penetration events, lipid flip-flop phenomena, and other characteristics of lipid membranes during the permeation of nanoparticles. The effect of ion concentration gradient, pressure differential across the membrane, nanoparticle size, and permeation velocity are examined. The findings from our work will lead to a better understanding of passive water and ion transport during permeation of nanoparticles and help in developing more efficient nanocarrier drug delivery systems while avoiding cell cytotoxicity.

2. METHODS

2.1. Coarse-Grained Model. A coarse-grained model allows us to extend the space and time scales of simulations compared to all-atom models. Coarse-grained (CG) models where small groups of atoms are treated as single beads provide a promising method to study large biomolecular systems.[29] Marrink and co-workers recently developed a coarse-grained force-field MARTINI for simulation of lipids and surfactants[30] and have extended it to amino acids and proteins.[31] The MARTINI force field has been shown to reproduce semiquantitatively fundamental structural and thermodynamic properties of lipid bilayers and proteins. The MARTINI force field[30] is one of the widely used coarse-grained (CG) models in MD simulations. More details about the MARTINI CG force field can be found in the literature.[30] Here, we will only describe the model briefly.

In the MARTINI CG model, all particle pairs i and j at distance r_{ij} interact via a Lennard-Jones (L-J) potential:

$$V_{LJ}(r_{ij}) = 4\varepsilon_{ij}\left[\left(\frac{\sigma_{ij}}{r_{ij}}\right)^{12} - \left(\frac{\sigma_{ij}}{r_{ij}}\right)^{6}\right] \quad (1)$$

The well depth ε_{ij} depends on the interacting particle types and values range from ε_{ij} = 5.6 kJ/mol for interactions between strong polar groups to ε_{ij} = 2.0 kJ/mol for interactions between polar and apolar groups, mimicking the hydrophobic effect. The effective size of particles is governed by the L-J parameter σ = 0.47 nm for all normal particle types, except that for the interaction between charged (Q type) and most apolar types (C1 and C2), the range of repulsion is extended by setting σ = 0.62 nm. In addition to the L-J interaction, charged groups interact via a shifted Coulombic potential function:

$$U_{elec} = \frac{q_i q_j}{4\pi\varepsilon_0\varepsilon_r r} \quad (2)$$

In the simulations described here, the nonbonded interactions are cut off at r_{cut} = 1.2 nm. The L-J potential is shifted from r_{shift} = 0.9−1.2 nm, and the electrostatic potential is shifted from r_{shift} = 0.0−1.2 nm following a standard shift function.[32]

The bonds are described by a harmonic potential $V_{bond}(R)$ and a cosine type harmonic potential $V_{angle}(\theta)$ is used for bond angles.

$$V_{bond}(R) = \frac{1}{2}K_{bond}(R - R_{bond})^2 \quad (3)$$

$$V_{angle}(\theta) = \frac{1}{2}K_{angle}\{\cos(\theta) - \cos(\theta_0)\}^2 \quad (4)$$

Because of the reduction in the degrees of freedom and elimination of fine interaction details, the dynamics of the coarse-grained simulation are observed to be accelerated by a constant amount, called the speed up factor, compared to the same system in all-atom representation. Usually, the time sampled using CG is 3−6 times larger than the atomistic models.[33] When interpreting the simulation results with the MARTINI CG model, Marrink et al. found that a factor of 4 appears to describe the general dynamics present in many membrane systems quite well.[33] Using this factor gives rates in good agreement with experiment and/or all-atom simulations for a variety of CG-simulated dynamic process.[33] Bennett et al. described simulations of lipid flip-flop by calculating the potential of the mean force using five different models varying from AA, bundled AA, CG (MARTINI), polarizable CG, and a CG model with a softer water potential in three different membranes.[34] Given the coarseness of the MARTINI model and the complexity of the flip-flop process and pore formation, the similarity in the PMFs found is encouraging.[34]

2.2. Simulation Setup. The lipid membrane system in the present work consists of 512 dipalmitoylphosphatidylcholine (DPPC) molecules and approximately 23 000 CG waters (4 water molecules in each CG water) in a 12.8 × 12.6 × 22.2 nm^3 simulation box. We have previously shown that this bilayer membrane self-assembles from an isotropic solution of lipids in CG simulations and that the properties of the self-assembled bilayers are in good agreement with experimental measurements, which validate the effectiveness of the coarse-grained model we are using for the lipid bilayers.[35]

To replicate the actual experiments in which the pore-spanning membrane was supported on a solid to prevent the entire membrane from moving, we simulated a solid support by tethering the boundary lipid molecules to their initial position with a harmonic spring force. Lipids 1 nm from each end (about 8% of the total membrane width, not the entire membrane) are tethered in our simulation system. We note that the simulation system we used here by design is not tension free, which may affect the permeation process. Two impermeable walls are inserted in our simulation system, separating the water phase into two independent compartments, as seen at the top and bottom of the simulation box in Figure 1. These two walls are impermeable to water and ions and are cut from a face-centered cubic (FCC) structure. To create a pressure differential across the membrane, the wall on the

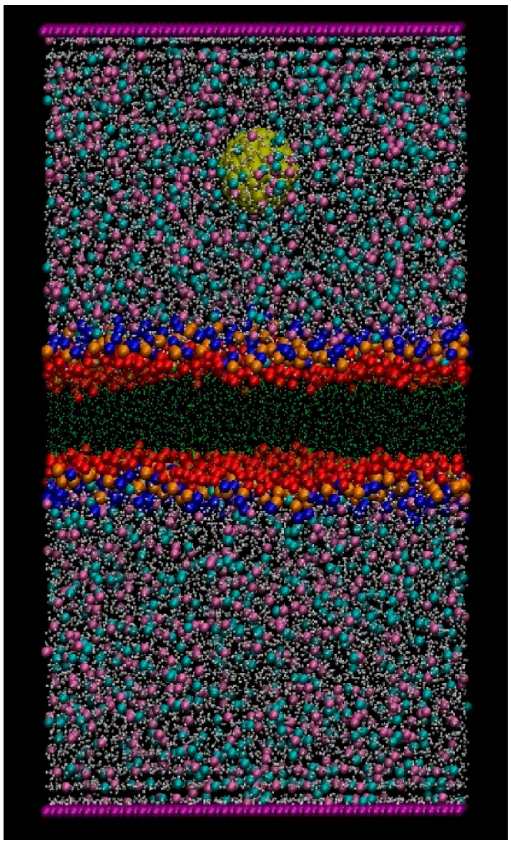

Figure 1. Simulation system for investigating the nanoparticle permeation induced water penetration, ion transport, and lipid flip-flop (blue represents the choline group, orange the phosphate group, red the glycerol group, green the tail group, yellow the gold nanoparticle, cyan represents the sodium ions, mauve dots are chloride ions, while purple dots are impermeable walls).

topside is moved toward the lipid bilayers at a velocity 0.025 m/s for 10 ns, and the system is then allowed to relax for another 10 ns for equilibrium. We created three pressure differentials by repeating this movement three times. The top wall is moved by a total distance of 0.75 nm, creating a maximum pressure differential of 300 bar between two sides of the lipid membrane. Our studies indicate that after 10 ns relaxation, the lipid membrane does not change significantly and appears to be close to equilibrium. For simulations involving ions, sodium and chloride ions are added to the water phase by replacing randomly chosen water molecules. We inserted 600 sodium and chloride ions in each water compartment, corresponding to a concentration of about 1.3 mol % (the saturation limit of salt in water is 1.8 mol %). We inserted an equal number of sodium and chloride ions in both water compartments to examine a system with no concentration gradient across the membrane (equal ion concentrations on both sides). In further studies, we only include sodium and chloride ions in the top compartment to examine systems with ion concentration gradients (unequal ion concentrations).

In our simulations, the interactions among the gold nanoparticles, ions, and lipid molecules are described by L-J potentials and the force field parameters from the standard MARTINI coarse-grained model. The classes of interaction sites and their accompanying potential parameters have previously been tested and verified against atomistic simulations by Marrink et al.,[30] and we have tested them in our simulation systems against experimental data for lipid membranes.[17] Various potential parameters have been used previously for gold atoms, from all-atom to coarse-grained (atomistic structure but modeling gold atoms as C-class[21] and P-class[36] using MARTINI force fields). Here, we assign MARTINI C5 type interaction sites for gold atoms. For the cross-interactions between gold nanoparticle and other interactive sites, we use the standard Lorentz−Berthelot mixing rules[37] as a starting point in this study. All the simulations were performed using the LAMMPS simulation package.[38] A Langevin thermostat[39] was applied in the NVT ensemble to maintain the desired temperature (323 K). To ensure stability, we used a time step of 10 fs. A typical simulation takes about 0.75 h per ns on an Intel Core2Quad CPU system.

After allowing equilibration of the system, we introduced one bare gold nanoparticle into our simulation system, as shown in Figure 1. The structure of the gold nanoparticle is obtained by cutting nearly spherical nanocrystals out of a bulk gold FCC lattice. In this study, various sizes of nanoparticle are investigated, from 1.0 to 4.0 nm in diameter. In practice, ligand-coated gold nanoparticles with a wide range of sizes in the range of 1−100 nm or more have been used for drug delivery and as imaging agents experimentally.[40] For example, Pan et al. have investigated the size dependence of the cell toxicity of water-soluble ligand-coated gold nanoparticles ranging from 0.8 to 15.0 nm in diameter.[41] Hainfeld et al.[42] used 1.9 nm AuNPs for imaging in mice. Thus, the sizes of our nanoparticles are of practical interest, although the present study uses bare gold nanoparticles. We have previously made detailed comparisons of membrane permeation by bare and ligand-coated nanoparticles.[17,18] We used an external force in the range of 50−1000 pN to aid the permeation of the nanoparticles in the membrane with velocity in the range 0.35−1.4 m/s[17,18] (The nanoparticle permeation velocities we examined here are 0.35, 0.525, 0.7, and 1.4 m/s respectively (velo1/2/3/4)). These external forces we applied are smaller than the forces for example between two nanoparticles −0 to 12 nN[43] or nanoparticles and cell membranes −50 to 1200 pN.[44] The nanoparticle velocities investigated (resulting from the forces applied) are larger than some experimental studies; these are however still several orders of magnitude smaller than the thermal velocities of water, ions, and lipid molecules (96.6−334.5 m/s) at the temperature investigated and an order of magnitude smaller than the nanoparticles (7.5 − 51.0 m/s). Therefore, we believe our simulations still represent the permeation process realistically, although the process has been facilitated to shorten the permeation time significantly due to computational constraints. This is also demonstrated by the recovery of the lipid layer between two permeation cycles indicating no permanent damage to the membrane even at these high velocities.[17] Others have used similar velocities and their results also appear in reasonable agreement with experiments.[45,46]

Hydrophobic nanoparticles often do accumulate in the lipid membrane; however, fully hydrophobic particles have also shown the ability to penetrate through the membrane under actual experimental conditions. For example, hydrophobic, chemically inert nanocrystals of corundum and quartz (spherical nanoparticles less than 15 nm in the size, like the nanoparticles we used in this work) have been experimentally observed to penetrate and exit the erythrocyte membranes.[47] In another experimental study, carbon nanotubes with a range of aspect ratios were reported to permeate plasma and nuclear membranes, without endocytosis.[48] The size of nanoparticles we used in our studies was smaller than the experimental studies (1−4 nm), as was the membrane thickness, so in an actual experimental system, permeation should be more likely in a system such as ours. The reason we must apply an external force has to do with the fact we only have one nanoparticle, and our simulation time by necessity must be smaller than that accessible experimentally. In many nanoparticle systems, interactions between nanoparticles may provide this force, and of course given enough time the random motion of the nanoparticle due to their high thermal velocity would ultimately enable these nanoparticles to permeate and exit the system, as has been observed experimentally. What we have done is biased the system with a uniform force well within the limits of the random Brownian force that NPs generally encounter.

In this study, the number of CG water molecules reported in the interior of the membrane corresponds to water molecules in the hydrophobic interior of the membrane. This region is defined as a slice extending 0.75 nm on either side of the center of the membrane. The water molecules located at the openings of the pore are therefore not counted. A penetration event is defined as the diffusion of an ion

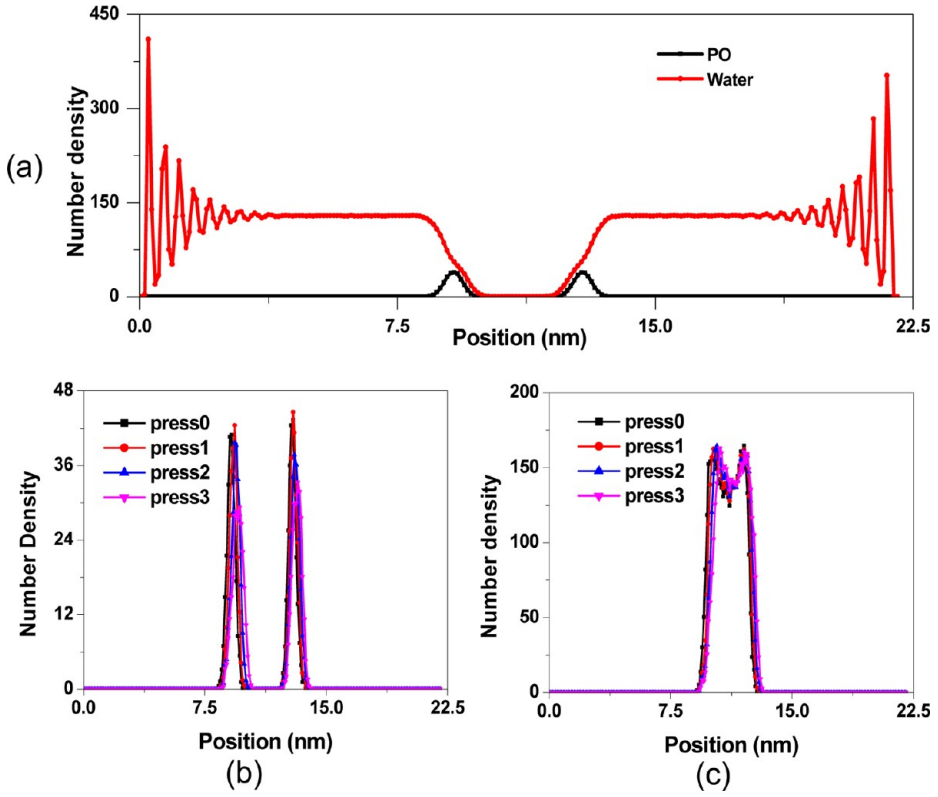

Figure 2. Density profiles of components of DPPC membrane and water molecules along the z direction. (a) Equilibrated lipid/water system after the insertion of two impermeable walls without compression. (b) Density profiles of phosphate groups under various compression. (c) Density profiles of tail groups under various compression.

moving from one boundary (defined by the average position of phosphate groups) in one layer to the other. Finally, we define a flip-flop occurrence as an event in which a lipid molecule moves from one leaflet of the bilayer to another. Lipid flip-flop is infrequently observed in fully intact bilayers due to the high free energy barrier involved in moving the polar head groups through the hydrophobic core. In intact planar-supported lipid bilayers, sum-frequency vibration spectroscopy has been used to measure the intrinsic rate of a flip-flop for bilayers consisting of protonated and perdeuterated lipids. An average free energy barrier for flip-flop of 220 kJ/mol for DPPC and two other lipids and 105 kJ/mol for DSPC was found.[49,50] This phenomenon has been observed experimentally during lipid fusion or under the perturbation of bilayer-disrupting peptides.[51] Electric pulses have also been shown to enhance the transbilayer mobility of phospholipids.[52]

3. RESULTS AND DISCUSSION

3.1. Lipid Membrane under Compression. The two walls we designed are impermeable to water or ions and the lipid bilayers are located at the center of the simulation box as seen in Figure 1. The equilibrated density profiles of phosphate groups and water molecules along the z-direction in the lipid/water system are shown in Figure 2a. The thickness of the lipid membrane, which is obtained from the distance between the phosphate groups, is 3.78 nm, in close agreement with the experimental value of 3.85 nm.[53] The upper impermeable wall was then moved toward the lipid bilayers to create the pressure differential in our simulation system. To maintain the stability of the system, low compression rates (0.025 m/s) and long relaxation times (10 ns) between each wall movement was used in this work. From the comparison of the density profile of phosphate group and tail group of the lipid membrane (Figure 2b,c) under various pressure differentials (press1/2/3) after the relaxation time compared with the original system (press0), the structure of the lipid membrane does not change significantly. The thickness of the lipid membrane shrinks by only 3.2% under a 300 bar pressure differential between the two sides of the membrane, which is shown in Table 1.

Table 1. Thickness of Lipid Membrane under Various Pressure Differentials

simulation system	thickness (nm)
press0	3.78
press1	3.74
press2	3.69
press3	3.66

3.2. Water Penetration. Microscopy experiments have examined the formation of nanoscale holes caused by nanoparticles in model membranes. For example, Chen et al. observed dendrimer nanoparticles making 3.0 nm diameter holes in living cell membranes.[54] In our previous simulation of the permeation of various sizes of nanoparticles (bare and ligand-coated nanoparticles) across the lipid membrane, we also observed the pore formation inside the membrane.[17,18] In the present study, we have focused on water penetration more comprehensively. We have investigated the dependence of water penetration on nanoparticle size, permeation velocity, pressure, and ion concentration gradient.

As is seen in Figure 3, water molecules start entering the lipid bilayer region when the nanoparticle touches the first layer of the membrane. The lipid molecules are compressed when the nanoparticle permeates the membrane, inducing defects in the interior of the membrane and a pore is therefore created. The

dx.doi.org/10.1021/la302879r | Langmuir 2012, 28, 16989−17000

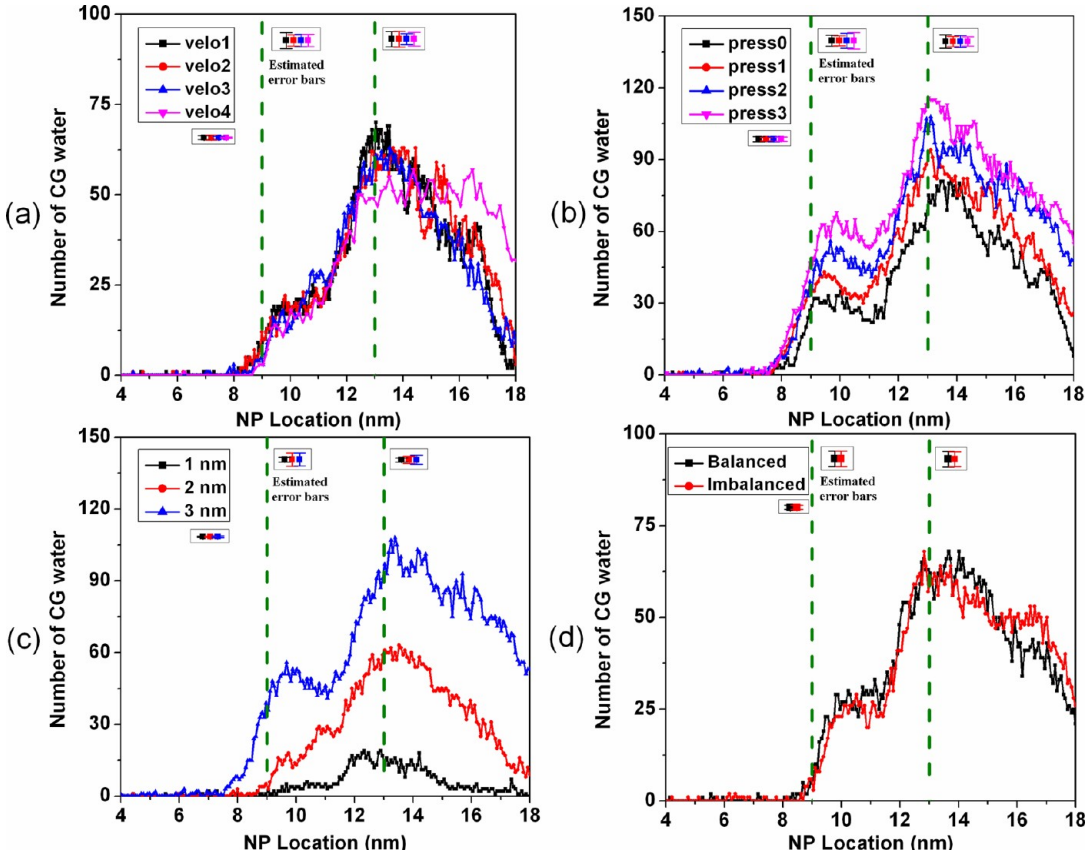

Figure 3. Number of water molecules in the interior of membrane under various conditions. (a) The nanoparticle permeation velocity effect, which is from 2.0 nm nanoparticles, no ion concentration gradient, and the press1 system. (b) The pressure effect, which is obtained from 3.0 nm nanoparticles, 0.7 m/s nanoparticle permeation velocity, and the ion concentration gradient system. (c) The size effect, which is obtained from no ion concentration gradient, 0.7 m/s nanoparticle permeation velocity, and the press2 system. (d) The ion concentration gradient effect, which is obtained from 2.0 nm nanoparticles, 0.7 m/s nanoparticle permeation velocity, and the press3 system. (The green dash line indicates the equilibrated position of the phosphate groups) Error bars in different regions are indicated on the graph.

number of water molecules entering the membrane increases as the nanoparticle moves through the membrane. The deeper the nanoparticle goes into the membrane, the more water molecules are observed. The number of water molecules penetrating the membrane is higher while the nanoparticle is permeating the headgroup of the first lipid bilayer. It slows down somewhat while it is permeating the tail region of the first bilayer. It increases significantly once more while the nanoparticle permeates the tail region of the second lipid bilayer. The structure of the lipid bilayer maintains its integrity until the nanoparticle starts permeating the second layer tail region. Once it enters this exiting region, the membrane structure is significantly disturbed as confirmed by the lipid order parameter. This then results in a significant increase in the pore size and the resultant water molecules inside the membrane. When the nanoparticle leaves the membrane and enters the second water phase, water molecules also move out of the membrane. This exit of water molecules results from the recovery of the membrane and the hydrophobicity of the lipid membrane interior.

The number of water molecules inside the membrane does not appear to be affected by the permeation velocity of the nanoparticle. However, the rate of recovery of the lipid membrane, as indicated by the exit of the water molecules from inside the membrane, increases with the nanoparticle permeation rate, as can be seen in Figure 3a. The smaller the permeation velocity, the easier for the lipid membrane to recover after the nanoparticle permeation. An increase in the pressure differential between the two sides of the membrane increases water penetration (Figure 3b). More water molecules enter the membrane interior when the nanoparticle is permeating under high-pressure differentials. The recovery of the membrane also slows down under larger pressure-differentials. Larger nanoparticles also lead to more water inside the lipid membrane, as seen in Figure 3c. In addition, larger nanoparticles disturb the internal structure of the membrane, which in turn elevates the changes in the local order parameter[17] and therefore makes it harder for the membrane to recover. Finally, we found that ion concentration gradients across the membrane as described in the studies below do not affect water penetration in the membrane (Figure 3d).

3.3. Ion Transport. We now examine ion transport induced by nanoparticle permeation. Because of the Coulombic interaction between charged lipid head groups and the ions and the hydrophobic properties inside the membrane, these ions get bound to the lipid head groups and are therefore unable to penetrate to the center of membrane on their own. The snapshots of a nanoparticle-mediated ion transport are shown in Figure 4. When the nanoparticle touches the membrane surface, some ions are pushed into the water/membrane interface, along with the deformation of the first layer and the formation of water pores inside the membrane. As the nanoparticle permeates farther inside the membrane, most

dx.doi.org/10.1021/la302879r | *Langmuir* 2012, 28, 16989−17000

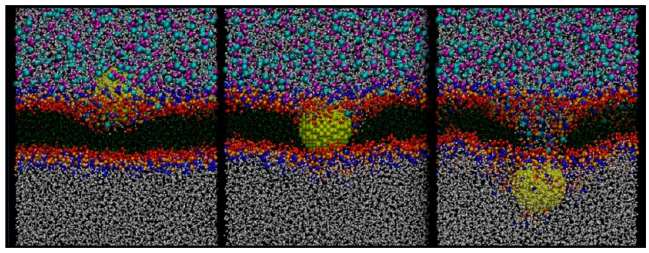

Figure 4. Snapshots for the water and ion translocation mediated by the nanoparticle permeation.

ions still return to the water/membrane interface, except for a few ions that continue to move along with the nanoparticle. These ions translocate to the center of the membrane once the nanoparticle moves completely across the first layer. Once the nanoparticle begins to enter the tail group of the second layer, as was reported earlier,[17] a larger pore is created inside the membrane. This increases the number of water molecules in the membrane, which also leads to a corresponding increase in the number of ions inside the membrane. The number of ions inside the membrane reaches its maximum value as the nanoparticle is exiting the membrane.

A summary of the 32 independent simulations to monitor the ion penetration events is presented in Table 2. An ion penetration event as described earlier is defined as the diffusion of an ion moving from one boundary that is the average position of phosphate groups in one layer to the other. Ion penetration is clearly sensitive to the size of nanoparticles. For diameters in the range of 1.0−4.0 nm, the number of permeation events increase exponentially as the size of nanoparticle increases. No ion penetration event is observed during the permeation of the 1.0 nm nanoparticle, which is not shown in Table 2. Larger nanoparticles increase the size of the created pore, which increases the incidence of penetration events for the ions. If we examine the case of no ion concentration gradient and press1 system as an example, 4 ion penetration events with a 2.0 nm nanoparticle, 14 for a 3.0 nm nanoparticle, while the number of penetration events reaches 119 with a 4.0 nm nanoparticle. With zero external pressure and no concentration gradient, we still observed ion penetration accompanying permeation of nanoparticles larger than 1.0 nm diameter.

Table 2. Summary of Ion Penetration Events under Various Conditions

size (nm)	concentration	pressure	velocity	Na^+	Cl^-
2	no gradient	press1	velo1	0	1
2	no gradient	press1	velo2	1	1
2	no gradient	press1	velo3	0	0
2	no gradient	press1	velo4	1	0
2	no gradient	press0	velo2	2	0
2	no gradient	press2	velo2	0	0
2	no gradient	press3	velo2	0	1
2	gradient	press1	velo1	0	0
2	gradient	press1	velo2	0	0
2	gradient	press1	velo3	1	1
2	gradient	press1	velo4	0	0
2	gradient	press0	velo2	2	0
2	gradient	press2	velo2	0	0
2	gradient	press3	velo2	0	0
3	no gradient	press1	velo1	1	2
3	no gradient	press1	velo2	2	3
3	no gradient	press1	velo3	2	2
3	no gradient	press1	velo4	2	0
3	no gradient	press0	velo2	2	2
3	no gradient	press2	velo2	2	2
3	no gradient	press3	velo2	3	2
3	gradient	press1	velo1	2	2
3	gradient	press1	velo2	1	4
3	gradient	press1	velo3	2	3
3	gradient	press1	velo4	2	2
3	gradient	press0	velo2	2	2
3	gradient	press2	velo2	4	3
3	gradient	press3	velo2	6	4
4	no gradient	press1	velo1	9	15
4	no gradient	press1	velo2	13	18
4	no gradient	press1	velo3	12	20
4	no gradient	press1	velo4	12	20

The equilibrated density profiles of sodium and chloride ions on both sides of the membrane in the absence of nanoparticles are shown in Figure 5. We observe that the sodium ion concentration peak is near the position of the phosphate group, while for chloride ions, a peak is observed in the interfacial layer near the membrane. The results in Table 2 do not show any selectivity for ions for penetration of nanoparticles up to 2.0 nm in size. This is most probably because the pores formed are not large enough for the hydrated ions, for all pressures and concentrations. For 3.0 nm particles, the nanoparticle permeation velocity does not appear to change the ion penetration events, as was observed in the case of water (see Figure 3a). In the case of unequal sodium chloride concentrations, the overall number of penetration events is larger compared to equal concentrations. The pores created here are large enough for hydrated ions to move inside the pore, so the additional chemical potential gradient due to unequal ion concentrations provides an additional driving force to facilitate ion transport. However, we do not observe any ion selectivity, either for 2.0 or 3.0 nm nanoparticle permeation. In the case of equal concentrations, pressure differentials do not appear to affect the ion penetration rate or selectivity. For the unequal concentrations, the overall ion penetration events increase significantly between the lowest pressure and higher pressures, but we do not observe any clear indication of selectivity. Therefore it appears that the combination of the chemical potential and hydrostatic driving force facilitates ion

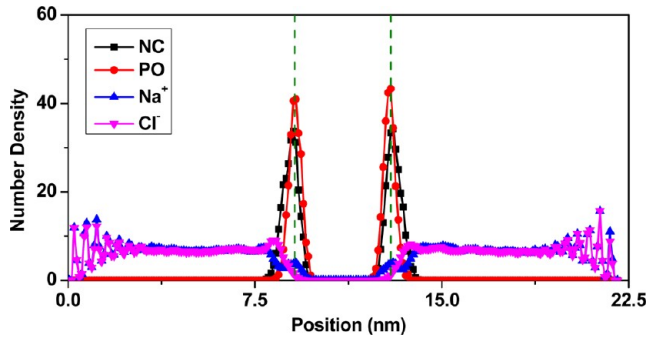

Figure 5. Density profiles of sodium and chloride ions, choline and phosphate groups of the equilibrated lipid/water/ion system along the z direction. (The green dashed line indicates the equilibrated position of phosphate groups in the unperturbed membrane).

dx.doi.org/10.1021/la302879r | *Langmuir* 2012, 28, 16989−17000

flow in the pores. In the absence of a chemical potential driving force, pressure differences alone cannot overcome the flow barriers in the transient pores created by the 3.0 nm particles permeating the membrane. With even larger particles, every factor that previously did not affect ion permeability or selectivity becomes important. For example for 4.0 nm particles, permeation velocity of the nanoparticle, which played no role previously, affects both the ion permeation rate and selectivity. There appears to be a bias for chloride transport. This has to do with the lower surface charge density of chloride ions which makes the hydrated ions more flexible, which enables chloride ions to more easily pass inside the pores formed. The latter behavior has been also observed in ion permeation of semirigid pores such as carbon nanotubes.[55] Simulations of ion permeation in preformed tension-stabilized pores in DPPC by Leontiadou et al.[11] also show that for larger pores (1.8 nm in radius), the chloride ion flux was an order of magnitude larger than that of the sodium ions.

Figure 6a shows typical ion trajectories for sodium and chloride ions, from which we see the sodium ions present a strong tendency to stay in the lipid membrane headgroup region once they get close to the first layer of the membrane, while chloride ions prefer to stay in the interfacial layer near the membrane. Once chloride ions touch the membrane, they quickly penetrate and cross the membrane. The average residence times for sodium and chloride ions inside the membrane are shown in Figure 6b. Although the residence time for both sodium and chloride ions have a wide variation, the residence times for sodium ions is much longer than for chloride ions. Such a kind of anionic selectivity has also been reported experimentally for large pores stabilized by specific cationic lipids[56] and theoretically from Leontiadou et al.'s work[11] and Gurtovenko's work,[13] in which the water pore is mediated by external electric fields and ion potential gradients.

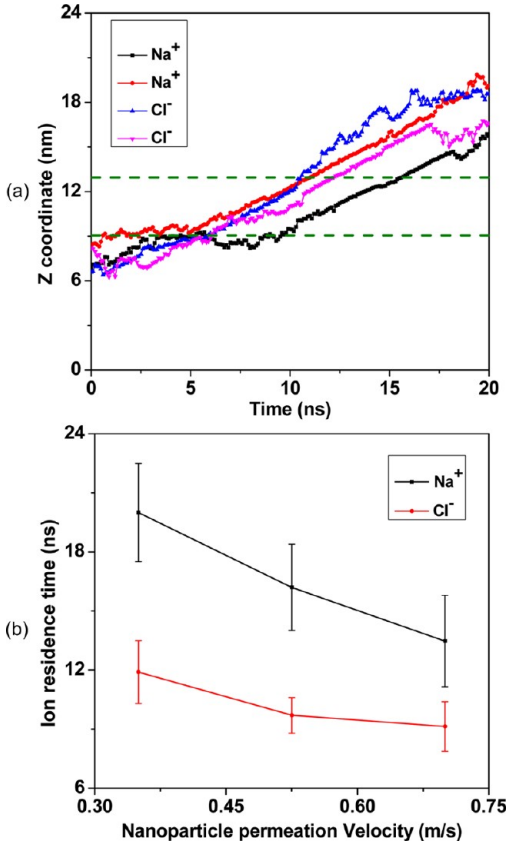

Figure 6. Typical Na^+ and Cl^- ion trajectories (a) and ion residence time (b) in the membrane during the nanoparticle permeation. (Green dashed line indicates the equilibrated position of phosphate group in the unperturbed membrane).

3.4. Lipid Flip-Flop. When a lipid molecule moves from one leaflet of the bilayer to another, it is said to have flip-flopped. The lipid molecule flip-flop phenomenon (transmembrane lipid translocation) is of significant biological importance because such a translocation process is involved in a variety of properties and functions of cell membranes, such as membrane asymmetry and stability,[57] modulation of the activity of membrane proteins,[58] and programmed cell death.[59] Molecular simulations can provide insight to understand the molecular mechanisms of such flip-flops. To complete the permeation of chemical species across a biological membrane, lipid molecule flip-flops may take place with the help of proteins or without them.[51] There are strong indications that lipid translocation across a lipid membrane is a pore-mediated process and that a major fraction of flip-flops takes place through defects in the lipid membranes.[60−63]

During the nanoparticle permeation process, we witness spontaneous translocation of lipid molecules from one membrane leaflet to another following the formation of a water-conducting pore inside the membrane. When the nanoparticle gets close to and begins to permeate into the membrane, the head groups of lipids in the first layer are compressed to make room for the nanoparticle cross-sectional area and the lipid tails are separated apart. At the same time, water molecules start to penetrate into the membrane, pushing some lipid molecules toward the center of the membrane. Those lipid molecules may therefore have a chance to cross the hydrophobic core region as part of the transient water-conducting pore. We found some lipid molecules undergo flip-flop events very quickly, while most of the flip-flopped lipid molecules spend some time to overcome the high free energy barrier involved in moving the polar head groups through the hydrophobic core. Nevertheless, our observations typified by the snapshots in Figure 7, on the basis of approximately 500 flip-flop events observed in all our simulations, indicate that lipid molecules undergoing the process progress through a series of similar-looking stages. As a lipid molecule moves along the z-direction from one layer to the other, an end-over-end molecular rotation occurs, during which the two alkyl tails open up and then come together again. The snapshots of six typical lipid molecule flip-flop events observed in our simulation are shown in Figure 7. In Figure 7a, we display 10 snapshots of a particular lipid undergoing a flip-flop. In the process, it undergoes conformational changes and overall rotation while translating along the z direction. In Figure 7b, each of the 5 lipid molecules being observed likewise translated along the z direction, but to save space we suppress the z translation in this part of the figure.

The water molecules in the transient pore play a role in the flip-flop events. Water interaction with the polar head groups assist in the process. The instantaneous number of water molecules in the interior of the membrane and the number of lipid molecules no longer present in their original layer are shown in Figure 8. The water molecules included in the count are those whose z coordinates are within 1.5 nm of the center of the membrane. The lipid molecules included in the count are those whose headgroup z coordinates are no longer within 3.0

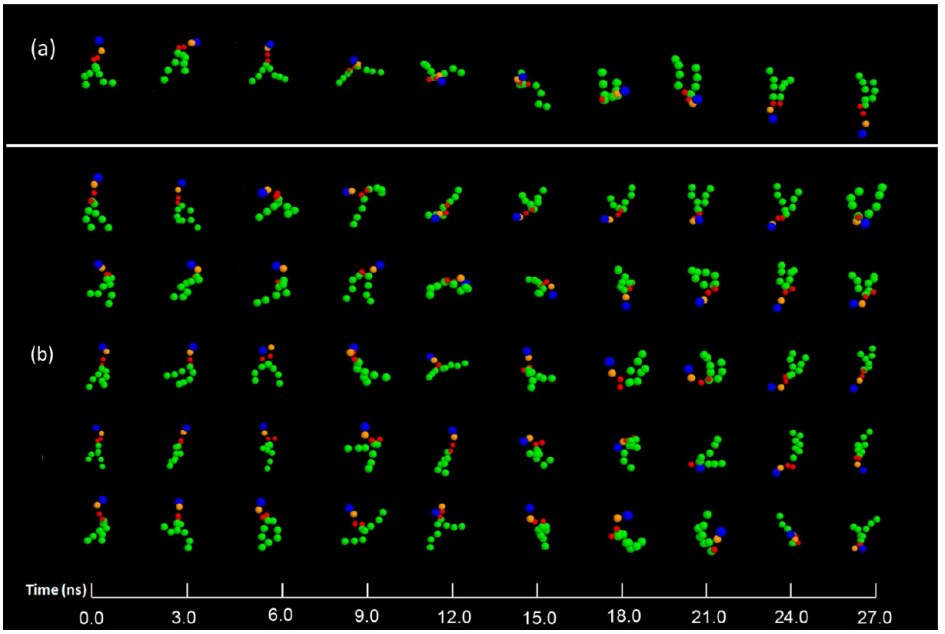

Figure 7. Snapshots of typical lipid molecule flip-flop events observed in our simulation, which are obtained from 3.0 nm nanoparticle permeation (0.525 m/s permeation velocity) under unequal ion concentration and press1 system.

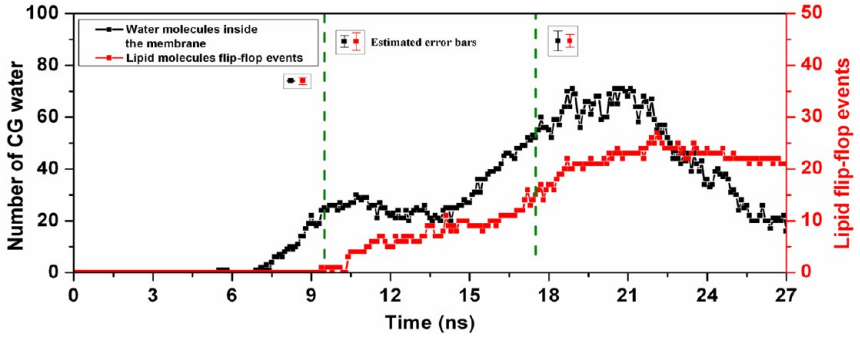

Figure 8. Number of water molecules in the interior of membrane and the instantaneous lipid molecule flip-flop events, which are obtained from 3.0 nm nanoparticle permeation (0.525 m/s permeation velocity) under an unequal ion concentration and the press1 system. (The green dashed line indicates the time during which the center of the nanoparticle is within the membrane.) Error bars in different regions are indicated on the graph.

nm of their original equilibrium position. The lipid flip-flop events start to show up when the nanoparticle permeates into the membrane. As the nanoparticle permeates deeper into the membrane, the number of flip-flop events increases, reaching their maximum where the water molecules in the interior of the membrane reach their maximum. In the snapshots in Figure 9, only the slice of the simulation box that includes the nanoparticles is shown for clarity, and only the lipid molecules (not water or ions) in the marked region are shown in the inset. These lipid molecules are in configurations typical of stages in the flip-flop process shown in Figure 7. This confirms our interpretation of the summary in Figure 8 that most of the flip-flop events occur in the "wake" of the nanoparticle with high incidence of water molecules inside the membrane accompanying the flip-flopping lipid molecules.

The stages in the mechanism of lipid flip-flop events we observed in our simulations are in agreement with the observations from atomistic simulations by Gurtovenko et al.,[28] where the lipid flip-flops in a preformed pore are induced by a transmembrane ion density gradient. Both "fast lipid flip-flops" (10–20 ns) and "slow flip-flops" (up to 130 ns) are observed in their simulations.[28] In our simulations, the time for

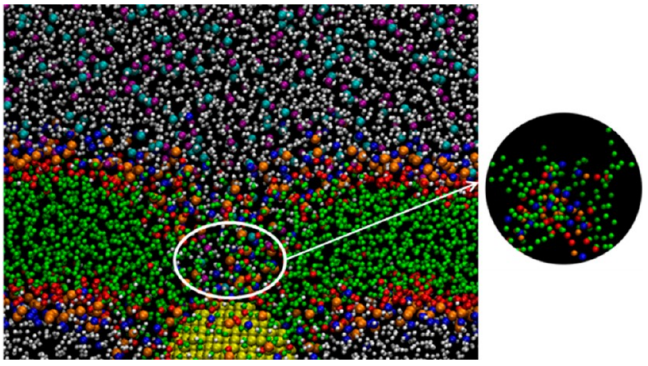

Figure 9. Snapshot showing lipid molecule flip-flops as the nanoparticle is moving out of the membrane. For clarity, only a section of the simulation box is shown. The inset shows only the lipid molecules in the marked region.

the lipid flip-flop relates to the nanoparticle permeation velocity because the occurrence of water-conducting pores in the membrane is caused by the permeation process of a nanoparticle. In a typical simulation run (a few examples are

dx.doi.org/10.1021/la302879r | *Langmuir* 2012, 28, 16989–17000

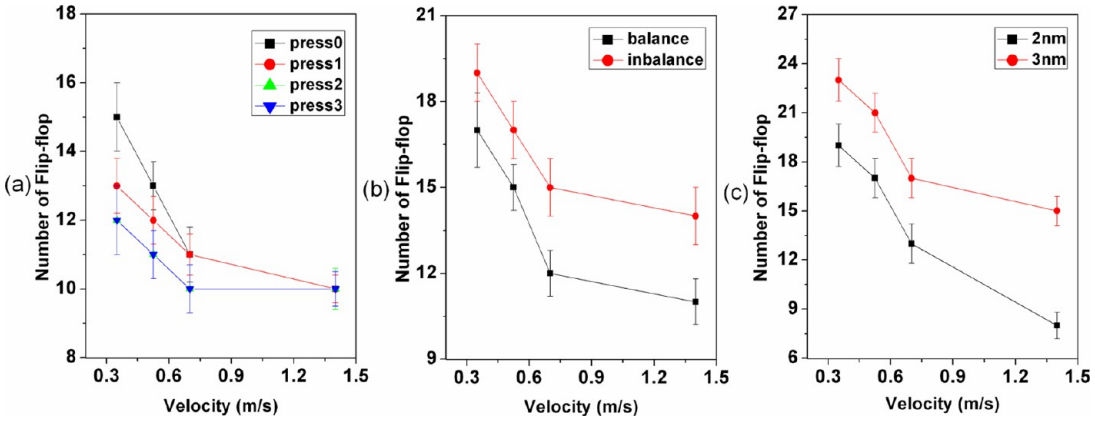

Figure 10. Lipid molecule flip-flop events under various conditions. (a) Effect of pressure differential and nanoparticle permeation velocity, which data is obtained from simulations with 2 nm nanoparticles and equal ion concentration. (b) Effect of potential gradient, which data is obtained from simulations with 3 nm nanoparticles under press2. (c) Effect of nanoparticle size, which data is obtained from simulations with unequal ion concentration under press1.

shown in Figure 7), the time for lipid molecule flip-flops varies from 3 to 27 ns, which is well in agreement with atomistic simulations if we consider the speed-up factor of 4 in our coarse-grained simulations.

We investigated how the number of incidences of flip-flops varies with conditions. Figure 10a–c summarizes the correlation of lipid flip-flop events observed with nanoparticle size, permeation velocity, pressure, and ion concentration differential. We found the number of lipid molecules that flip-flop decreases as we increase the nanoparticle permeation velocity (Figure 10a). Larger permeation velocities lead to shorter lifetime of pores in the interior of the membrane, which diminishes the available time for such flip-flops. As seen in Figure 11, the lifetime of the transient pore decreases

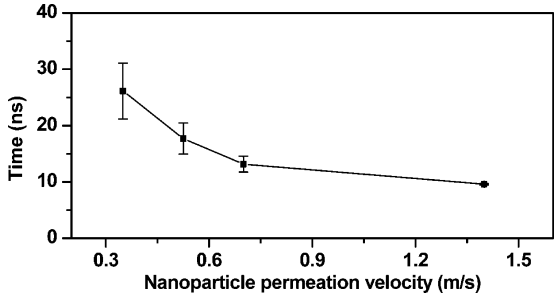

Figure 11. Pore lifetime as a function of nanoparticle permeation velocity (data obtained from simulations with 2.0 nm nanoparticles under equal ion concentrations).

significantly when the permeation velocity is below 0.7 m/s, while there is no significant change when the permeation velocity is above 0.7 m/s. We therefore observed that when the permeation velocity is over 0.7 m/s, for most cases, the number of lipid flip-flops reach a limiting value and no longer change with velocity. The number of lipid flip-flops decreases with the pressure differential between two sides of the membrane (Figure 10a). Although the penetration of water molecules increases as the pressure increases, higher pressures lower the mobility of the lipid molecules because of membrane compression, making flip-flops less frequent. As seen in Figure 10b,c, the number of flip-flopped lipid molecules is affected by the ion concentration differential and the size of the nanoparticle. A concentration gradient between two sides of the membrane, as shown earlier, facilitates ion transport through the water pore. Such ion transport quickly discharges the transmembrane ionic charge imbalance and makes the water pore more stable,[13] which can lead to enhanced flip-flops. Also, with larger diameter nanoparticles, higher water and ion penetration is observed; both in turn increase the number of lipid molecule flip-flops that occur.

3.5. After the Permeation. It is known that the permeation of nanoparticles and the accompanying water and ion flux can affect the stability and the mechanical strength of lipid membranes.[64] It is therefore important to understand if and how a membrane recovers following the nanoparticle permeation. We have investigated the thickness, order parameter, and related properties to understand the nature of any permanent changes, if any, occur following the nanoparticle permeation. To observe the recovery of the lipid membrane, we held the nanoparticle in place and continued the simulation for an additional 10 ns after the nanoparticle has permeated the lipid membrane and reached the other side. (This was accomplished by stopping the movement of the nanoparticle and tethering it at the bottom end of the system, see Figure 1.) We refer to the property averages obtained in the additional 10 ns as "at the end" and the property averages for the equilibrated unperturbed membrane as "at the beginning".

The thickness of the lipid membrane begins to increase once the nanoparticle reaches the surface of the lipid membrane, compared to its equilibrium undisturbed condition. After the nanoparticle moves into the membrane, the thickness of the membrane increases quite significantly from its equilibrium value. Larger nanoparticles induce more perturbations in the lipid membrane, resulting in a greater increase in the thickness. In all the simulations we have carried out here, we observed that the thickness of the lipid membrane completely recovers after permeation by a nanoparticle, which confirms the healing ability of membranes. Figure 12 shows the density profiles of phosphate and tail groups at the beginning and at the end in two typical simulations (Case1, 2 nm nanoparticle, 0.7 permeation velocity, equal ion concentration and press3 system; Case2, 3 nm nanoparticle, 1.4 m/s permeation velocity, unequal ion concentration, and press1 system). The density profiles for phosphate and tail groups change slightly after the nanoparticle permeation. This is expected since lipid membranes have been observed to self-assemble even from

dx.doi.org/10.1021/la302879r | *Langmuir* 2012, 28, 16989–17000

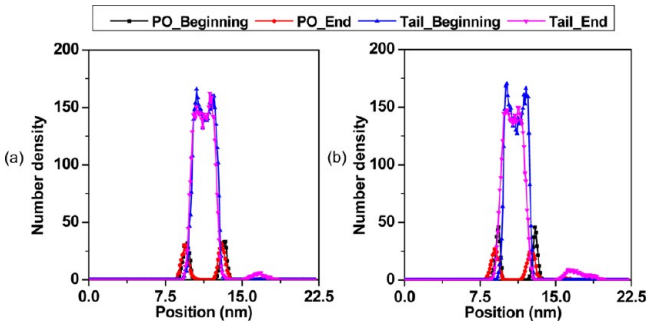

Figure 12. Comparison of density profiles of phosphate and tail groups of DPPC membrane along the *z* direction at the beginning of the simulation and at the end of the simulation after tethering the nanoparticle for 10 ns. (a) Case 1: simulation system with 2 nm nanoparticles, 0.7 m/s permeation velocity, equal ion concentration, and the press3 system. (b) Case 2: simulation system with 3 nm nanoparticles, 1.4 m/s permeation velocity, unequal ion concentration, and the press1 system.

an initial random configuration of lipids in solution in our work. We witnessed a few lipid molecules being dragged out to the bulk solution, making the bare nanoparticles appear as a ligand-coated nanoparticle. This explains the small peak observed in the density profile (Figure 12) of phosphate and tail groups at the end of our simulations.

We also monitored the tail segment order parameter. The order parameter is slightly larger during the nanoparticle permeation, compared to the unperturbed lipid membrane, which is consistent with our previous work.[17] This is due to the decrease of the dynamic space for the lipid membrane after the insertion of the nanoparticle, which induces lower mobility and lesser extent of isotropic averaging for lipid molecules of the entire lipid bilayer. However, 10 ns after the particle has permeated, the order parameter reverts back to the unperturbed value, as indicated from two typical simulations (Case 1, 2 nm nanoparticle, 0.7 permeation velocity, equal ion concentration, and press3 system; Case 2, 3 nm nanoparticle, 1.4 m/s permeation velocity, unequal ion concentration, and press1 system) in Figure 13. Since the lipid molecules had been individually tagged, we found a small fraction of the first layer lipids in the second layer and vice versa, after recovery of the membrane. Since both layers had the same lipid composition to start with, this leads to no net change in the lipid composition

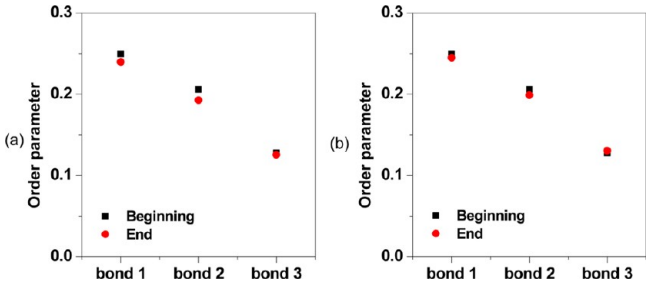

Figure 13. Comparison of tail segment order parameter of DPPC membrane at the beginning of the simulation and at the end of the simulation after tethering the nanoparticle for 10 ns. (a) Case 1: simulation system with 2 nm nanoparticles, 0.7 m/s permeation velocity, equal ion concentration, and the press3 system. (b) Case 2: simulation system with 3 nm nanoparticles, 1.4 m/s permeation velocity, unequal ion concentration, and the press1 system.

of the two layers. The structural changes in the membrane can be monitored by tracking the membrane thickness, membrane deformation, area per lipid, lipid order parameter, lipid tail length, and so on. These changes were reported in our previous work.[17] Overall, the membrane shows excellent recovery to its original structure.

4. CONCLUSIONS

Nanoparticles are generally considered excellent candidates for targeted drug delivery. However, ion leakage and cytotoxicity induced by nanoparticle permeation is a potential problem in such drug delivery schemes because of the toxic effect of many ions. A series of coarse-grained molecular dynamics simulations has been carried out to investigate the water and ion penetration and lipid molecule flip-flop in a protein-free phospholipid bilayer membrane during nanoparticle permeation. The effect of ion concentration gradient, pressure differential across the membrane, nanoparticle size, and permeation velocity have been examined in this work.

We found the number of water molecules in the membrane during the nanoparticle permeation increases with the nanoparticle size and with the pressure differential across the membrane but is unaffected by the nanoparticle permeation velocity or the ion concentration gradient. Ion penetration is sensitive to the size of the nanoparticle as well as the ion concentration gradient between two sides of the membrane; no anion/cation permeation is found under small nanoparticle permeation (1.0 nm); anion selectivity arises when the size of the nanoparticle reaches 4.0 nm. We also investigated lipid molecule flip-flop phenomena during the nanoparticle permeation. We found the number of lipid molecule flip-flops increases with the size of the nanoparticle and the ion concentration gradient, while it decreases with the pressure differential and the nanoparticle permeation velocity. The ability of the lipid membrane to recover has been demonstrated under the various conditions we have examined in this work. Lipid flip-flop events have been demonstrated accompanying nanoparticle penetration of lipid bilayers membranes. There is no resulting net change in lipid composition of the two layers in the case of symmetrical bilayers. However, biological lipid membranes have mixed compositions and are inherently asymmetrical in the two layers. Passage of nanoparticles across the biological membrane will therefore result in changing the compositions of both inner and outer layers, which may have some physiological consequences. The findings described in this work leads to a better understanding of passive water and ion transport and lipid flip-flops during the permeation of nanoparticles and should help in developing more efficient nanocarrier drug delivery systems while avoiding cell cytotoxicity.

AUTHOR INFORMATION

Corresponding Author

*E-mail: murad@uic.edu. Phone: (312)-996-5593.

Notes

The authors declare no competing financial interest.

ACKNOWLEDGMENTS

This research has been funded by a grant from the Office of Basic Energy Science, Department of Energy (Grant No. DE-FG02-08ER4653) and the National Science Foundation (Grant No. CBET-0730026).

REFERENCES

(1) Bonting, S. L.; De Pont, J. J. H. H. M. *Membrane Transport*; Elsevier/North-Holland Biomedical Press: Amsterdam, The Netherlands, 1981.

(2) Toyoshima, Y.; Thompson, T. E. Chloride flux in bilayer membranes - chloride permeability in aqueous dispersions of single-walled bilayer vesicles. *Biochemistry* **1975**, *14*, 1525−1531.

(3) Deamer, D. W.; Bramhall, J. Permeability of lipid bilayers to water and ionic solutes. *Chem. Phys. Lipids* **1986**, *40*, 167−188.

(4) Tepper, H. L.; Voth, G. A. Protons may leak through pure lipid bilayers via a concerted mechanism. *Biophys. J.* **2005**, *88*, 3095−3108.

(5) Nel, A.; Xia, T.; Madler, L.; Li, N. Toxic potential of materials at the nanolevel. *Science* **2006**, *311*, 622−627.

(6) Goodman, C. M.; McCusker, C. D.; Yilmaz, T.; Rotello, V. M. Toxicity of gold nanoparticles functionalized with cationic and anionic side chains. *Bioconjugate Chem.* **2004**, *15*, 897−900.

(7) Sayes, C. M.; Liang, F.; Hudson, J. L.; Mendez, J.; Guo, W. H.; Beach, J. M.; Moore, V. C.; Doyle, C. D.; West, J. L.; Billups, W. E.; Ausman, K. D.; Colvin, V. L. Functionalization density dependence of single-walled carbon nanotubes cytotoxicity in vitro. *Toxicol. Lett.* **2006**, *161*, 135−142.

(8) Roiter, Y.; Ornatska, M.; Rammohan, A. R.; Balakrishnan, J.; Heine, D. R.; Minko, S. Interaction of nanoparticles with lipid membrane. *Nano Lett.* **2008**, *8*, 941−944.

(9) Gurtovenko, A. A.; Anwar, J.; Vattulainen, I. Defect-mediated trafficking across cell membranes: Insights from in silico modeling. *Chem. Rev.* **2010**, *110*, 6077−6103.

(10) Tepper, H. L.; Voth, G. A. Mechanisms of passive ion permeation through lipid bilayers: Insights from simulations. *J. Phys. Chem. B* **2006**, *110*, 21327−21337.

(11) Leontiadou, H.; Mark, A. E.; Marrink, S. J. Ion transport across transmembrane pores. *Biophys. J.* **2007**, *92*, 4209−4215.

(12) Kandasamy, S. K.; Larson, R. G. Cation and anion transport through hydrophilic pores in lipid bilayers. *J. Chem. Phys.* **2006**, *125* (7), 074901.

(13) Gurtovenko, A. A.; Vattulainen, I. Ion leakage through transient water pores in protein-free lipid membranes driven by transmembrane ionic charge imbalance. *Biophys. J.* **2007**, *92*, 1878−1890.

(14) Lawaczeck, R. Deffect structures in membranes- routes for the permeation of small molecules. *Phys. Chem. Chem. Phys.* **1988**, *92*, 961−963.

(15) Jansen, M.; Blume, A. A comparative study of diffusive and osmotic water permeation across bilayers composed of phospholipids with different head groups and fatty acyl chains. *Biophys. J.* **1995**, *68*, 997−1008.

(16) Hamilton, R. T.; Kaler, E. W. Alkali metal ion transport through thin bilayers. *J. Phys. Chem.* **1990**, *94*, 2560−2566.

(17) Song, B.; Yuan, H.; Jameson, C. J.; Murad, S. Permeation of nanocrystals across lipid membranes. *Mol. Phys.* **2011**, *109*, 1511−1526.

(18) Song, B.; Yuan, H.; Jameson, C. J.; Murad, S. Role of surface ligands in nanoparticle permeation through a model membrane: a coarse-grained molecular dynamics simulations study. *Mol. Phys.* **2012**, *110*, 2181−2195.

(19) Yang, K.; Ma, Y. Q. Computer simulation of the translocation of nanoparticles with different shapes across a lipid bilayer. *Nat. Nanotechnol.* **2010**, *5*, 579−583.

(20) Fiedler, S. L.; Violi, A. Simulation of nanoparticle permeation through a lipid membrane. *Biophys. J.* **2010**, *99*, 144−152.

(21) Lin, J.; Zhang, H.; Chen, Z.; Zheng, Y. Penetration of lipid membranes by gold nanoparticles: Insights into cellular uptake, cytotoxicity, and their relationship. *ACS Nano* **2010**, *4*, 5421−5429.

(22) Qiao, R.; Roberts, A. P.; Mount, A. S.; Klaine, S. J.; Ke, P. C. Translocation of C-60 and its derivatives across a lipid bilayer. *Nano Lett.* **2007**, *7*, 614−619.

(23) Prates Ramalho, J. P.; Gkeka, P.; Sarkisov, L. Structure and phase transformations of DPPC lipid bilayers in the presence of nanoparticles: insights from coarse-grained molecular dynamics simulations. *Langmuir* **2011**, *27*, 3723−30.

(24) Van Lehn, R. C.; Alexander-Katz, A. Penetration of lipid bilayers by nanoparticles with environmentally-responsive surfaces: simulations and theory. *Soft Matter* **2011**, *7*, 11392−11404.

(25) Li, Y.; Gu, N. Computer simulation of the inclusion of hydrophobic nanoparticles into a lipid bilayer. *J. Nanosci. Nanotechnol.* **2010**, *10*, 7616−7619.

(26) Ding, H.; Ma, Y. Interactions between Janus particles and membranes. *Nanoscale* **2012**, *4*, 1116−1122.

(27) Ding, H.; Tian, W.; Ma, Y. Designing nanoparticle translocation through membranes by computer simulations. *ACS Nano* **2012**, *6*, 1230−1238.

(28) Gurtovenko, A. A.; Vattulainen, I. Molecular mechanism for lipid flip-flops. *J. Phys. Chem. B* **2007**, *111*, 13554−13559.

(29) Nielsen, S. O.; Lopez, C. F.; Srinivas, G.; Klein, M. L. Coarse grain models and the computer simulation of soft materials. *J. Phys.: Condens. Matter* **2004**, *16*, 481−512.

(30) Marrink, S. J.; Risselada, H. J.; Yefimov, S.; Tieleman, D. P.; de Vries, A. H. The MARTINI force field: Coarse grained model for biomolecular simulations. *J. Phys. Chem. B* **2007**, *111*, 7812−7824.

(31) Monticelli, L.; Kandasamy, S. K.; Periole, X.; Larson, R. G.; Tieleman, D. P.; Marrink, S. J. The MARTINI coarse-grained force field: Extension to proteins. *J. Chem. Theory Comput.* **2008**, *4*, 819−834.

(32) Baron, R.; de Vries, A. H.; Hunenberger, P. H.; van Gunsteren, W. F. Configurational entropies of lipids in pure and mixed bilayers from atomic-level and coarse-grained molecular dynamics simulations. *J. Phys. Chem. B* **2006**, *110*, 15602−15614.

(33) Marrink, S. J.; de Vries, A. H.; Mark, A. E. Coarse grained model for semiquantitative lipid simulations. *J. Phys. Chem. B* **2004**, *108*, 750−760.

(34) Bennett, W. F. D.; Tieleman, D. P. Water defect and pore formation in atomistic and coarse-grained lipid membranes: pushing the limits of coarse graining. *J. Chem. Theory Comput.* **2011**, *7*, 2981−2988.

(35) Yuan, H.; Jameson, C. J.; Murad, S. Diffusion of gases across lipid membranes with OmpA channel: a molecular dynamics study. *Mol. Phys.* **2009**, *108*, 1569−1581.

(36) Hofler, L.; Gyurcsanyi, R. E. Coarse grained molecular dynamics simulation of electromechanically-gated DNA modified conical nanopores. *Electroanalysis* **2008**, *20*, 301−307.

(37) Maitland, G. C., R., M., Smith, E. B., Wakeham, W. A., *Intermolecular Forces: Their Origin and Determination*; Oxford University Press: New York, 1987.

(38) Plimpton, S. Fast parallel algorithms for short-range molecular dynamics. *J. Comput. Phys.* **1995**, *117*, 1−19.

(39) Schneider, T.; Stoll, E. Molecular dynamics study of a 3-dimensional one-component model for distortive phase-transitions. *Phys. Rev. B* **1978**, *17*, 1302−1322.

(40) Tiwari, P.; Vig, K.; Dennis, V.; Singh, S. Functionalized gold nanoparticles and their biomedical applications. *Nanomaterials* **2011**, *1*, 31−63.

(41) Pan, Y.; Neuss, S.; Leifert, A.; Fischler, M.; Wen, F.; Simon, U.; Schmid, G.; Brandau, W.; Jahnen-Dechent, W. Size-dependent cytotoxicity of gold nanoparticles. *Small* **2007**, *3*, 1941−1949.

(42) Hainfeld, J. F.; Slatkin, D. N.; Smilowitz, H. M. The use of gold nanoparticles to enhance radiotherapy in mice. *Phys. Med. Biol.* **2004**, *49*, 309−315.

(43) Zeng, Q.; Yu, A.; Lu, G. Evaluation of interaction forces between nanoparticles by molecular dynamics simulation. *Ind. Eng. Chem. Res.* **2010**, *49*, 12793−12797.

(44) Vasir, J. K.; Labhasetwar, V. Quantification of the force of nanoparticle-cell membrane interactions and its influence on intracellular trafficking of nanoparticles. *Biomaterials* **2008**, *29*, 4244−4252.

(45) Lee, O. S.; Schatz, G. C. Computational simulations of the interaction of lipid membranes with DNA-functionalized gold nanoparticles. *Methods Mol. Biol.* **2011**, *726*, 283−96.

(46) Wallace, E. J.; Sansom, M. S. P. Blocking of carbon nanotube based nanoinjectors by lipids: A simulation study. *Nano Lett.* **2008**, *8*, 2751−2756.

(47) Mokrushnikov, P.; Panin, L.; Zaitsev, B.; Doronin, N.; Kozelskaya, A.; Panin, A. Interaction of corundum and quartz nanocrystals with erythrocyte membranes. *Biophysics* **2011**, *56*, 1074−1077.
(48) Nagai, H.; Okazaki, Y.; Chew, S. H.; Misawa, N.; Yamashita, Y.; Akatsuka, S.; Ishihara, T.; Yamashita, K.; Yoshikawa, Y.; Yasui, H.; Jiang, L.; Ohara, H.; Takahashi, T.; Ichihara, G.; Kostarelos, K.; Miyata, Y.; Shinohara, H.; Toyokuni, S. Diameter and rigidity of multiwalled carbon nanotubes are critical factors in mesothelial injury and carcinogenesis. *Proc. Natl. Acad. Sci. U.S.A.* **2011**, *108*, 1330−1338.
(49) Liu, J.; Conboy, J. C. 1,2-diacyl-phosphatidylcholine flip-flop measured directly by sum-frequency vibrational spectroscopy. *Biophys. J.* **2005**, *89*, 2522−2532.
(50) Anglin, T. C.; Cooper, M. P.; Li, H.; Chandler, K.; Conboy, J. C. Free energy and entropy of activation for phospholipid flip-flop in planar supported lipid bilayers. *J. Phys. Chem. B* **2010**, *114*, 1903−1914.
(51) Raggers, R. J.; Pomorski, T.; Holthuis, J. C. M.; Kalin, N.; van Meer, G. Lipid traffic: The ABC of transbilayer movement. *Traffic* **2000**, *1*, 226−234.
(52) Schwarz, S.; Haest, C. W. M.; Deuticke, B. Extensive electroporation abolishes experimentally induced shape transformations of erythrocytes: a consequence of phospholipid symmetrization. *Biochim. Biophys. Acta, Biomembr.* **1999**, *1421*, 361−379.
(53) Nagle, J. F.; Zhang, R. T.; TristramNagle, S.; Sun, W. J.; Petrache, H. I.; Suter, R. M. X-ray structure determination of fully hydrated L(alpha) phase dipalmitoylphosphatidylcholine bilayers. *Biophys. J.* **1996**, *70*, 1419−1431.
(54) Chen, J. M.; Hessler, J. A.; Putchakayala, K.; Panama, B. K.; Khan, D. P.; Hong, S.; Mullen, D. G.; DiMaggio, S. C.; Som, A.; Tew, G. N.; Lopatin, A. N.; Baker, J. R.; Holl, M. M. B.; Orr, B. G. Cationic nanoparticles induce nanoscale disruption in living cell plasma membranes. *J. Phys. Chem. B* **2009**, *113*, 11179−11185.
(55) Liu, H.; Murad, S.; Jameson, C. J. Ion permeation dynamics in carbon nanotubes. *J. Chem. Phys.* **2006**, *125* (8), 084713.
(56) Chanturiya, A.; Yang, J. P.; Scaria, P.; Stanek, J.; Frei, J.; Mett, H.; Woodle, M. New cationic lipids form channel-like pores in phospholipid bilayers. *Biophys. J.* **2003**, *84*, 1750−1755.
(57) Manno, S.; Takakuwa, Y.; Mohandas, N. Identification of a functional role for lipid asymmetry in biological membranes: Phosphatidylserine-skeletal protein interactions modulate membrane stability. *Proc. Natl. Acad. Sci. U.S.A.* **2002**, *99*, 1943−1948.
(58) Pomorski, T.; Hrafnsdottir, S.; Devaux, P. F.; van Meer, G. Lipid distribution and transport across cellular membranes. *Semin. Cell Dev. Biol.* **2001**, *12*, 139−148.
(59) Balasubramanian, K.; Schroit, A. J. Aminophospholipid asymmetry: A matter of life and death. *Annu. Rev. Physiol.* **2003**, *65*, 701−734.
(60) Tieleman, D. P.; Marrink, S. J. Lipids out of equilibrium: Energetics of desorption and pore mediated flip-flop. *J. Am. Chem. Soc.* **2006**, *128*, 12462−12467.
(61) de Vries, A. H.; Mark, A. E.; Marrink, S. J. Molecular dynamics simulation of the spontaneous formation of a small DPPC vesicle in water in atomistic detail. *J. Am. Chem. Soc.* **2004**, *126*, 4488−4489.
(62) Dickey, A. N.; Faller, R. How alcohol chain-length and concentration modulate hydrogen bond formation in a lipid bilayer. *Biophys. J.* **2007**, *92*, 2366−2376.
(63) Leontiadou, H.; Mark, A. E.; Marrink, S. J. Antimicrobial peptides in action. *J. Am. Chem. Soc.* **2006**, *128*, 12156−12161.
(64) Jiang, W.; Kim, B. Y. S.; Rutka, J. T.; Chan, W. C. W. Nanoparticle-mediated cellular response is size-dependent. *Nat. Nanotechnol.* **2008**, *3*, 145−150.